Geomorphology 438 (2023) 108826

Contents lists available at ScienceDirect

Geomorphology

journal homepage: www.journals.elsevier.com/geomorphology

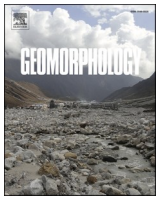

Total water level controls on the trajectory of dune toe retreat

Matthew P. Conlin [a,b,*,1], Nicholas Cohn [b], Peter N. Adams [a]

[a] Department of Geological Sciences, University of Florida, Gainesville, FL, USA
[b] Coastal and Hydraulics Laboratory – Field Research Facility, U.S. Army Engineer Research and Development Center, Duck, NC, USA

ARTICLE INFO

Keywords:
Lidar
Storms
Coastal foredunes
Dune toe retreat trajectory
Total water level

ABSTRACT

This study examines the trajectory (slope) of coastal foredune toe retreat in response to nine storm events that impacted the Outer Banks, North Carolina, USA. High resolution, three-dimensional, repeat mobile terrestrial lidar observations over a four kilometer stretch of coast were used to assess spatiotemporal beach and dune evolution at the storm timescale. Consistent with existing field observations from other sandy coastlines, an upward toe retreat was observed for most instances of dune retreat in the Outer Banks. However, these new topographic data indicate that the retreat can proceed steeply downward when the maximum total water level (TWL) defined by the 2% runup exceedance level is not high enough, for long enough, to erode the dune face. Non-linear relationships were found between the dune toe retreat trajectory as well as both the magnitude and duration of TWL above the dune toe, where instances of upward- and downward-directed retreat are best differentiated using the 7% runup exceedance level, rather than the commonly used 2% level. This physically justified non-linear relationship is shown to be consistent with observations from other studies, and could be a more effective parameterization for the retreat trajectory than those currently implemented in wave-impact dune erosion models.

1. Introduction

Coastal foredunes represent depositional landforms that have formed in response to interactions between sediment, wind, waves, and ecological processes (Psuty, 2004; Durán and Moore, 2013). The local topographic high of the foredune has often been described as a critical "last line of defense" for backshore communities from storm-driven waves and elevated water levels (Carter, 1991; Palmsten and Holman, 2012; Brodie et al., 2019; Jackson et al., 2019; Davidson et al., 2020). This recognition has led to an increasing occurrence of dune construction and planting on managed coastlines to increase coastal resilience to storms and climate change (Martínez et al., 2013; Jackson and Nordstrom, 2020). Foredunes also provide important ecosystem services (McLachlan, 1991; Frank, 1996) and recreational value (Drius et al., 2019). Knowledge of foredune response to storms is therefore critical for protecting coastal communities and habitats in the face of a changing climate, yet this understanding remains incomplete (Davidson et al., 2020).

The potential for a storm to impact a dune is often conceptualized through comparison of the maximum height of the storm-induced total water levels (TWL), which are defined as the sum of lunar tides, non-tidal residuals such as storm surge, and wave runup (e.g. Serafin et al., 2017), relative to the height of the foredune crest and toe. Under the Storm Impact Scale (SIS) model of Sallenger (2000), four dune impact regimes of variable severity are defined. In the 'collision regime', wave runup impacts the dune face above the dune toe, but does not exceed the height of the dune crest. When in this regime, surf-zone processes may temporarily replace swash conditions on the upper beach, promoting beach and dune erosion through turbulence-induced sediment entrainment and subsequent offshore transport driven by backwash and undertow (Masselink and Puleo, 2006; Stockdon et al., 2007; Masselink and van Heteren, 2014). As a result, upper beach erosion commonly coincides with collisional impacts (Stockdon et al., 2007; Coco et al., 2014; Masselink and van Heteren, 2014; Dissanayake et al., 2015; Burvingt et al., 2017; Héquette et al., 2019; Cohn et al., 2019; Davidson et al., 2020). The impacts of swash and/or short waves on the dune face during dune collision also commonly generates dune scarps (e.g. van Rijn, 2009; De Winter et al., 2015; Suanez et al., 2015; Houser et al., 2018; Davidson et al., 2020; Cohn et al., 2021). Infiltration of swash into the dune via capillary action acts as a destabilizer by increasing the

* Corresponding author.
E-mail address: conlinm@oregonstate.edu (M.P. Conlin).
[1] Present address: College of Earth, Ocean, and Atmospheric Science, Oregon State University, Corvallis, OR, USA.

https://doi.org/10.1016/j.geomorph.2023.108826
Received 7 February 2023; Received in revised form 7 July 2023; Accepted 7 July 2023
Available online 9 July 2023

effective weight of dune sediment, thereby decreasing slope stability (Palmsten and Holman, 2011), causing blocks to slump from the face. In response to direct short wave impact, scarping may occur as a result of layer separation along vertical cracks that develop, slumping of material overlying a wave-cut notch at the base of the dune, or sliding of material off the dune face as surficial sediment is removed from the base (Nishi and Kraus, 1996).

While the relationship between storm-induced water levels relative to the dune face geometry plays a first order control on foredune response, numerous other physical attributes of the dune have been shown to be important for driving the magnitude and style of dune retreat (e.g. Davidson et al., 2020). For example, vegetation roots, stems, and mycorrhiza can all stabilize dune sediments and attenuate flow velocity/shear stress which may reduce potential for dune erosion in response to a given TWL forcing (Carter, 1980; Feagin et al., 2015; Maximiliano-Cordova et al., 2019). Similarly, increasing dune sediment compaction decreases dune erodibility (Nishi and Kraus, 1996). Partial saturation of sediment also results in a compressive force that acts to increase cohesion between sediment grains and reduce dune erodibility (McCarthy, 1977). Nearshore, beach and foredune morphology also exert an important control on dune response to a storm, for example through the morphology of a crescentic outer bar (Castelle et al., 2015, 2016), anomalously deep nearshore features (Cohn et al., 2021), beach slope/width (Saye et al., 2005; Burroughs and Tebbens, 2008; Fernandez et al., 2011; Splinter et al., 2014; Cohn et al., 2018, 2019), and sediment grain size (Masselink and Puleo, 2006). Further, these nearshore, beach, and dune morphologic controls may be tied to previous storm impacts; for example, through existing overwash channels that act to channelize flows during the next event and promote further dune erosion (Houser et al., 2008), or nearshore bars developed during one event that act to dissipate wave energy and buffer the beach from further erosion during the next (Vousdoukas et al., 2012). In this way, morphologic signatures left by one event can influence response to subsequent events, illustrating that storm response cannot be considered in isolation, but rather previous response/recovery intervals must be taken into account (Masselink and van Heteren, 2014; Conlin et al., 2020).

Numerous numerical tools of various complexity have been developed to simulate the timing and magnitude of dune erosion during storms. The conceptual storm impact scale (SIS) is among the simplest of these tools, where beach/dune response is inferred from the four impact regimes rather than being explicitly quantified. Notably, SIS regimes are typically calculated using the elevation exceeded by 2 % of runup events ($R_{2\%}$; e.g. Stockdon et al., 2007). However, it has been suggested that less extreme elevation thresholds, such as $R_{16\%}$, are nearly as or more effective than $R_{2\%}$ for predictions of dune erosion volume (Palmsten and Holman, 2012; Splinter and Palmsten, 2012). The effectiveness of different runup exceedance levels in terms of predictions of dune erosion will be further tested in this work. On the other end of the complexity spectrum, various models aim to resolve wave-averaged or wave-resolved physics to simulate sediment transport over the entire cross shore profile (e.g. CSHORE; Kobayashi, 2016 and XBeach; Roelvink et al., 2009). An intermediate, parametric approach is the wave impact approach, wherein the rate of volumetric dune erosion is modeled to be proportional to the wave momentum flux impacting the dune (Overton and Fisher, 1988; Overton et al., 1994; Larson et al., 2004; Palmsten and Holman, 2012). Wave-impact dune erosion models, developed from laboratory studies, simulate dune retreat along an unchanging trajectory of the toe (β_T) that is parameterized as a direct linear function of the beach face slope (β_f); i.e. $\beta_T \propto \beta_f$ (Larson et al., 2004; Palmsten and Holman, 2012). Though field observations of β_T are limited, those that exist have called into question this universal linear parameterization in terms of β_f (Bonte and Levoy, 2015; Overbeck et al., 2017). Observed longshore varying β_T/β_f ratios have been shown to span values of 0.54 to 2.54 from measurements from Australian (Splinter and Palmsten, 2012), French (Bonte and Levoy, 2015), and United States (Brodie and Spore, 2015) coasts. This range suggests an upward dune toe trajectory, whereby the post-storm dune toe elevation is higher than the pre-storm dune toe elevation, is common, although the magnitude of β_T could potentially be either steeper or shallower than β_f. Most recently, Overbeck et al. (2017) examined β_T in response to hurricane Sandy at over 800 cross-shore transects along the northern U.S. mid-Atlantic coast. They found that β_T was similar to β_f at only half of their locations. At the other half, the dune toe retreated downward (post-storm toe lower in elevation than pre-storm toe), indicating that a model using a constant direct parameterization in terms of β_f would obtain large errors in 50 % of locations. These studies collectively indicate that other morphological or environmental processes may be responsible for dictating the magnitude and sign of β_T, but those factors have yet to be explored.

In this study, we aim to further investigate the potential morphological and/or environmental controls on β_T using new datasets of storm-induced dune response associated with nine storm events along the Outer Banks of North Carolina, U.S.A. For each event, β_T is quantified alongside changes to beach and dune volumes and morphology, and these are interpreted in the context of storm-driven TWL.

2. Study area

The study area is a four km stretch of exposed sandy coastline along the Outer Banks of North Carolina located in the southeastern U.S.A. (Fig. 1a). The U.S. Army Engineer Research and Development Center's (ERDC) Field Research Facility (FRF) property represents the southernmost 1 km of our study area (i.e. Y = 0–1000 m; Fig. 1b). The study area and surrounding Outer Banks are wave dominated barrier islands that are generally considered to be of intermediate beach type in the Wright and Short (1984) classification scheme, with steep beach slopes that are on the order of 0.10 with a standard deviation of approximately 0.02 (Birkemeier, 1985; Lee et al., 1998; Madsen and Plant, 2001). Grain size is variable spatially and temporally, though the local average grain size is ~0.3 mm (Cohn et al., 2022a). The lower beach is often influenced by beach cusp formation and evolution (O'Dea and Brodie, 2019). Wave heights during quiescent conditions are ~1 m (Birkemeier, 1985), though as will be shown herein, nearshore significant wave heights can exceed 5 m during storms. The tide is semidiurnal with a typical range of ~1 m (Lee et al., 1998).

A prominent dune was constructed along the entirety of the North Carolina Outer Banks in the 1930s–40s (Birkemeier et al., 1984). No active management has occurred on the dune within the FRF property (Y = 0–1000 m) since construction. However, north of the property, the beach and dune are actively managed through beach nourishment and dune vegetation planting, including a beach nourishment conducted during the study period which was completed just weeks before the impact of Maria (2017). Within the FRF property, the dunes in the northern section have been eroding since 2000, including a retreat of 25 m from 2003 to 2014 and ~1 m between 2015 and 2017, but the dunes in the southern section have vertically accreted and prograded over the same interval (Brodie et al., 2019; Cohn et al., 2022b). Dune heights within the property and the rest of the study site generally reach 6–8 m elevation (relative to NAVD88), while dune toes are typically at ~3–4 m (e.g., Brodie and Spore, 2015). The four km domain was chosen (1) because there is frequent topographic data from this entire stretch as part of a regular remote sensing-based coastal monitoring program and (2) there is generally considerable alongshore variability in observed beach properties (beach slope, grain size, dune toe/crest elevation) within this stretch despite similar offshore forcing conditions over this limited alongshore length scale.

The study area sees frequent storms throughout much of the year (Dolan et al., 1988). During the late summer and fall, tropical cyclones moving up the Atlantic coast commonly impact the site (Dolan and Davis, 1994). In the fall and winter months, the meeting of Arctic air

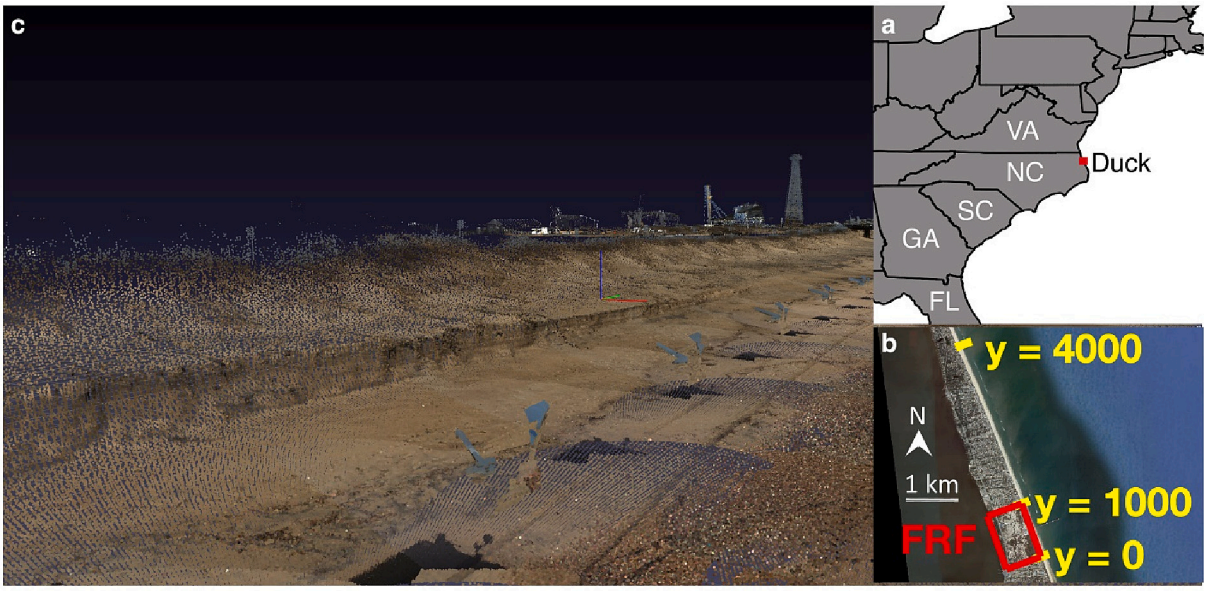

Fig. 1. Study site and data. (a) Location of site on the Atlantic coast of the U.S. (b) Satellite image of the site showing the location of the FRF property and longshore coordinate locations. (c) Example colorized point cloud from the Coastal Lidar and Radar Imaging System.

with the warm waters of the Gulf Stream off of North Carolina forms low pressure systems called Nor'Easters (often abbreviated NE in this work) that also impact the site (Dolan and Davis, 1992; Brodie et al., 2019). Both storm classes can drive elevated waves and water levels at the site.

3. Methods

3.1. Beach and dune morphology observations

Observations of beach and dune morphology have been collected regularly in the vicinity of the FRF since 2011 using the Coastal Lidar and Radar Imaging System (CLARIS; Cohn et al., 2022b). The CLARIS system includes a Riegl VZ-2000 terrestrial Lidar scanner, inertial measurement unit (IMU), and global positioning system (GPS) mounted atop a vehicle (currently a van). As the vehicle drives alongshore, the Lidar collects in framescan mode, creating a 3-d point cloud as it progresses (Spore and Brodie, 2017). The resulting seamless point cloud of the dry beach and foredune face achieves typical point densities of 75–100 points/m^2 (Spore and Brodie, 2017). The point cloud is filtered to remove non-ground points (vegetation, structures) using algorithms within RiScanPro and the resulting morphology observations are accurate to around 0.08 m in the horizontal and 0.10 m in the vertical (Spore and Brodie, 2017).

All available CLARIS datasets were searched to find survey pairs that were conducted within a few weeks before and after a storm event. This first involved finding survey pairs separated by at most a few weeks, followed by a qualitative examination of intervening wave conditions to determine if a storm occurred. A total of 13 pre/post-storm survey pairs were found, spanning the time period 2011–2021 (Table 1). These datasets were then further examined to remove those that do not encompass the study area and/or where data quality issues prevent a reliable extraction of the dune toe. This resulted in the removal of four survey pairs, yielding a total of 9 survey pairs spanning 2013–2021 used for analysis (Table 1). Four survey pairs bracketed Nor'Easter events and five bracketed hurricanes: Maria (2017), Riley (2018), Dorian (2019), Humberto (2019), and Teddy (2020) (Table 1). Note that the survey pair encompassing Hurricane Riley does not capture the northernmost 200 m of the study area.

Table 1
Summary of CLARIS pre/post-storm survey pairs used for this work.

Survey (pre)	Survey (post)	Days between	Storm	Used?	Reason(s) for rejection
2011-08-25	2011-08-29	4	Irene	x	Data do not cover study area Data do not capture dune
2013-03-06	2013-03-20	14	NE[a]	✓	N/A
2016-08-26	2016-09-13	18	Hermine	x	Data do not cover study area
2017-09-18	2017-09-22	4	Jose	x	Data do not cover study area Missing data on mid-beach
2017-09-22	2017-09-29	7	Maria	✓	N/A
2018-03-03	2018-03-09	6	Riley[b]	✓	N/A
2019-09-04	2019-09-10	6	Dorian	✓	N/A
2019-09-10	2019-09-24	14	Humberto	✓	N/A
2019-10-11	2019-10-15	4	NE	✓	N/A
2019-11-14	2019-11-19	5	NE	✓	N/A
2020-03-05	2020-03-10	5	NE	x	Data do not cover study area
2020-09-10	2020-09-25	15	Teddy	✓	N/A
2021-03-18	2021-03-23	5	NE	✓	N/A

[a] NE indicates Nor'Easter.
[b] No data in northern-most 200 m of study area.

3.2. Automated extraction of dune retreat and dune toes

For each survey, the filtered CLARIS point cloud was rotated and translated to a local standardized FRF coordinate system (oriented cross-shore and alongshore) and cropped to the study area. The rotation angle used was −20° true north. The cropped point clouds were gridded into digital surface models (DSMs) at 0.5 m × 0.5 m resolution. Gridding of

the multi-million point clouds was accomplished through a simple nearest neighbor approach, where the elevation of each grid node was taken as the minimum elevation of all data points for which that node is closest. Additionally, cross shore profiles were extracted from the rotated and cropped point cloud at 5 m alongshore spacing. Profiles were extracted using a cross-shore moving average window of 0.25 m applied to all observations within 2.5 m of the profile location.

Instances of dune retreat from each pre/post storm survey pair were automatically extracted using the DSMs and cross-shore profiles with a heuristic rules-based approach. An instance of dune retreat was extracted as a spatially continuous region at least 25 m in longshore length where bed lowering of at least 0.5 m occurred somewhere above a minimum pre-storm elevation of 2 m. The resulting change regions could include those only within the dune, those only on the beach (though reaching above 2 m elevation), and/or areas in between. To ensure each region described dune retreat, regions were further checked after dune toes were extracted on cross-shore profiles (see below); any profile location at which the region of bed lowering was entirely seaward of the pre-storm dune toe was removed. Further, to prevent artifacts due to data uncertainty and/or profile interpolation, only profiles at which the dune toe is found to have retreated by at least 0.5 m were considered.

Dune toe cross-shore location (X_{Toe}) and elevation (Z_{Toe}) were automatically extracted from the cross-shore profiles. Though the definition of the dune toe can vary based on background and sub-discipline, it is often defined in terms of a peak in curvature along the cross-shore profile (Smith et al., 2020). Following this common definition of Z_{Toe} utilized in similar studies of dune impact (Stockdon et al., 2007; Palmsten and Holman, 2012; Brodie and Spore, 2015; Overbeck et al., 2017; Smith et al., 2020), a maximum curvature approach was used here. Profiles were first linearly resampled to 1 m cross-shore spacing (to remove high spatial frequency noise), and (X_{Toe}, Z_{Toe}) was extracted as the point of maximum curvature on the resampled profile between 2 and 5 m elevation. While variable alongshore and through time, Z_{Toe} at this site typically occupies elevations between 3 and 4 m (e.g., Brodie and Spore, 2015).

3.3. Dune change morphometrics

At each profile within the extracted regions of dune retreat, the dune toe retreat trajectory (β_T) was quantified (Fig. 2). β_T is defined as the negative slope (dimensionless) between the pre- and post-storm dune toe positions, and is therefore calculated as:

$$\beta_T = -\frac{Z_{Toe}\,(post) - Z_{Toe}\,(pre)}{X_{Toe}\,(post) - X_{Toe}\,(pre)}. \tag{1}$$

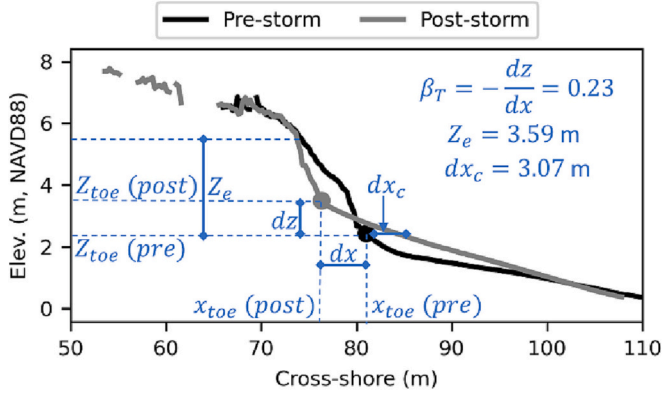

Fig. 2. Definition sketch for dune change morphometrics: dune toe retreat trajectory (β_T), maximum height above the pre-storm dune toe that erosion occurred (Z_e), and change in dune toe contour position (dx_c). Dots represent dune toes.

The sign convention is such that positive values of β_T indicate upward dune toe retreat (toe moving landwards and increasing in elevation) and negative values of β_T indicate downward retreat (toe moving landwards and decreasing in elevation; e.g. Fig. 2). Note that this sign convention is opposite that which has generally previously been used (e.g. Palmsten and Holman, 2012; Overbeck et al., 2017), though is adopted here for intuition. To provide further context for the β_T values, other parameters were also calculated (Fig. 2): Z_e, the maximum elevation to which dune erosion occurred, relative to Z_{Toe} (pre) (units of m); and dx_c, the horizontal change in the position of the pre-storm dune toe contour (units of m).

3.4. Wave and water level observations and metrics

Wave observations were obtained from the Waverider buoy offshore from the FRF property located in 17.8 m of water. This is one of at least 4 inshore wave buoys deployed along a cross-shore transect at Y = 960 m and stretching from the surf-zone to 26 m water depth. The buoy returns time series of significant wave height (H_s), spectral peak wave period (T_p) and wave direction (D, true north) sampled at half hourly intervals. Note that missing data in 2013 were replaced using similar observations from the buoy located in 26 m water depth transformed to 17.8 m depth using linear wave theory assuming shore parallel contours. Water level observations were obtained at hourly intervals from a tide gauge located at the end of a pier on the FRF property (Y = 500 m) that protrudes seaward 560 m into the Atlantic Ocean.

Total water level (TWL) was quantified at hourly intervals using the wave and water level observations. TWL was calculated following Serafin et al. (2017) as the sum of the measured still water level (SWL) and wave runup (R):

$$TWL = SWL + R. \tag{2}$$

R, being composed of wave setup elevation and swash elevation, is often calculated using the Stockdon et al. (2006) formulation, which provides the elevation exceeded by 2 % of runup events ($R_{2\%}$). Palmsten and Holman (2012) note that, assuming a mostly gaussian relationship between swash and runup elevation, this formulation can be modified to calculate runup with different elevation exceedance values (n%) by modifying the number of swash standard deviations considered:

$$R_{n\%} = 1.1\left(0.35\beta_f (H_0 L_0)^{1/2} + \frac{\left[H_0 L_0\left(0.563\beta_f^2 + 0.004\right)\right]^{1/2}}{2}\frac{n_\sigma}{2}\right), \tag{3}$$

where H_0 is the offshore wave height, L_0 the offshore wave length, and n_σ is the number of standard deviations of swash considered. For dune erosion studies, β_f is often calculated as the average slope between the dune toe and mean high water contour (MHW; e.g. Palmsten and Holman, 2012; Stockdon et al., 2012; Mull and Ruggiero, 2014; Cohn et al., 2019; Cohn et al., 2021). We follow this convention in our calculations of alongshore-variable β_f, however many cross-shore profiles extracted from CLARIS do not reach as low as MHW (0.36 m NAVD); when profiles do not reach MHW, β_f is calculated as the average slope between the dune toe and the farthest offshore point on the profile in order to remain as consistent with previous studies as possible. Note that, given the method of beach profile extraction given in Section 3.2, the β_f at each profile represents a 5 m alongshore average centered on the profile location.

The first term in Eq. (3) represents the wave setup, and the second represents the swash elevation modified to account for different n_σ. For example, $n_\sigma = 2$ considers two standard deviations of swash elevation, providing the elevation exceeded by 2 % of runup events ($R_{2\%}$; as in Stockdon et al., 2006). Similarly, $n_\sigma = 1.5$ provides the elevation exceeded by 7 % of runup events ($R_{7\%}$), $n_\sigma = 1$ provides the elevation exceeded by 16 % of runup events ($R_{16\%}$), etc. Note also that $n_\sigma = 0$

provides the *TWL* calculated with the mean runup level, that is, calculated to the location of time-averaged wave setup. This vertical level is also referred to as the dynamic still water level (DSWL; Cohn et al., 2019). We calculate *TWL* using different n_σ values, and we will refer to these values hereafter as $TWL_{m\%}$ using the corresponding m. For example, *TWL* calculated with $n_\sigma = 1$ will be referred to as $TWL_{16\%}$, representing the elevation exceeded by 16 % of runup events.

Extending the concept of *TWL* freeboard, defined as the difference between the *TWL* and the dune crest elevation (Long et al., 2014; Overbeck et al., 2017), here we define the dune toe freeboard ($F_{T,m\%}$) as the relative difference between the $TWL_{m\%}$ and the local Z_{Toe}. We further define the impact duration ($t_{I,m\%}$) as the amount of time for which $F_{T,m\%}$ was >0 m, or equivalently for which $TWL_{m\%}$ was above Z_{Toe}. Here, $F_{T,m\%}$ and $t_{I,m\%}$ are calculated following Eq. (3) using three different elevation exceedance values: $TWL_{2\%}$, $TWL_{7\%}$, and $TWL_{16\%}$, corresponding to $F_{T,2\%}$, $t_{I,2\%}$; $F_{T,7\%}$, $t_{I,7\%}$; and $F_{T,16\%}$, $t_{I,16\%}$; respectively.

4. Results

4.1. Storm-driven waves and water levels

2013NE and Riley produced the largest H_s of the analyzed storms, both exceeding 5 m at their peak. Maria, Dorian, 2019NE2, Teddy, and 2021NE all produced maximum H_s between 4 and 5 m, while Humberto and 2019NE1 produced smaller maximum H_s of <3.5 m. Riley also produced the longest T_p (>15 s) and the highest reference $TWL_{2\%}$ (i.e. assuming a uniform β_f of 0.1) of 4.16 m (Fig. 3, Table 2), and the largest reference DSWL of 2.39 m. No other storm generated a reference $TWL_{2\%}$ >3.7 m, however all others except Humberto, including 2019NE1, produced a reference $TWL_{2\%}$ >2.9 m (Table 2). Riley, Dorian, and 2019NE2 produced surge of at least 0.7 m, with Dorian producing the largest at 0.9 m (Table 2). 2019NE1, Teddy, and 2019NE2 generated surge of at least 0.5 m, while 2013NE, Maria, and Humberto did not. Additionally, for each storm the largest waves generally coincide with the most northerly wave directions, except for 2019NE2 (Fig. 3). On average, waves from most storms approached from nearly shore normal (70°), with Dorian driving the largest relative wave angle on average (19°; Table 2). 2019NE2 also resulted in relatively high angle waves at 13°; all other storms were within 11° (Table 2).

4.2. Storm-driven dune retreat

Fig. 4 presents pre- and post-storm profiles at two example transect locations: one in the unmanaged dune (Y = 200 m; Fig. 4a) and one in the managed dune (Y = 1900; Fig. 4b). A large offshore translation of the profile at Y = 1900 m between post-2013NE and pre-Maria (2017) totaling 60 m at the 1 m elevation contour is evident and represents sediment additions related to a beach and dune nourishment project conducted along a subset of the area of interest (Y > 1000 m) and finished just weeks before Maria's impact. Additionally, in general, large storm-driven changes are evident on the beach. For example, the erosion of berms during Teddy and Riley. In contrast, little change is apparent in the upper dunes on the storm timescale. The interface between beach and dune, the dune toe, appears to be a dynamic feature which sometimes retreated upwards (e.g. 2021NE at both transects, Riley at Y = 1900 m) and sometimes downwards (e.g. 2019NE2 at Y = 1900 m). These patterns are explored in more quantitative detail next.

Instances of dune retreat were automatically extracted from maps of bed elevation change (Appendix 1) as spatially continuous regions of at least 25 m in the longshore where bed lowering of at least 0.5 m occurred somewhere above a minimum pre-storm elevation of 2 m, and further checked using the profile observations. Zones of dune retreat were measured in response to seven of the nine storms considered,

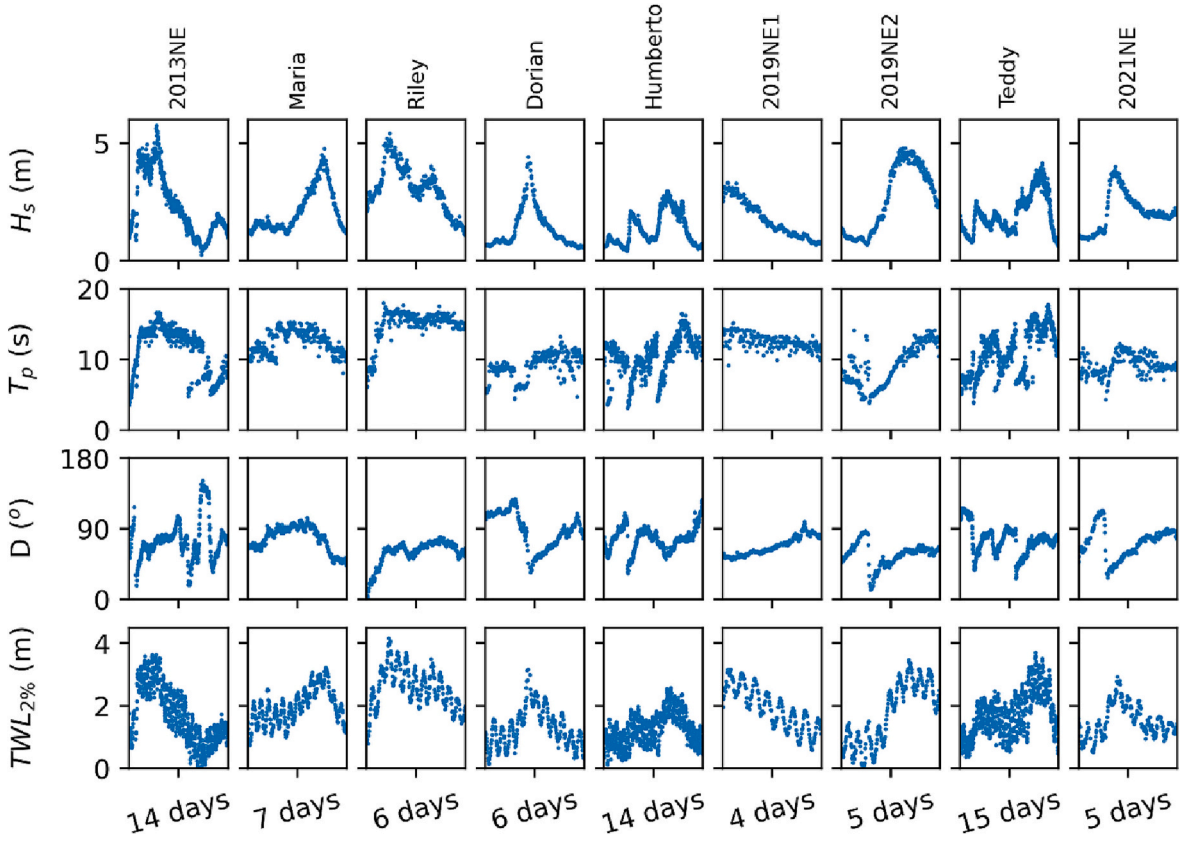

Fig. 3. Wave and water level observations for each storm. Each storm is a column. Total water level calculation ($TWL_{2\%}$) assumes a spatially uniform beach slope of 0.1.

Table 2
Summary of hydrodynamic and morphologic forcing parameters for each storm.

	Max reference $TWL_{2\%}$ (tide|surge|runup) (m)[a,b]	Max reference DSWL (m)[a]	Max H_s (m)	D ($\mu \pm 1\sigma$) (°)	$Z_{toe}(pre)$ ($\mu \pm 1\sigma$) (m)	Pre-storm β_f ($\mu \pm 1\sigma$)	Rainfall (mm)[c]
2021NE	2.92 (0.23|0.61|2.09)	1.71	4.01	72.63±19.54	3.42±0.62	0.08±0.03	25.40
Teddy	3.69 (0.70|0.50|2.48)	2.24	4.15	76.00±17.65	3.42±0.78	0.07±0.03	38.5
2019NE2	3.46 (0.50|0.70|2.27)	2.14	4.79	57.55±14.90	3.64±0.88	0.09±0.02	13.20
2019NE1	3.16 (0.41|0.51|2.25)	1.85	3.32	67.83±11.73	3.54±0.73	0.11±0.02	25.40
Humberto	2.58 (0.48|0.36|1.74)	1.56	2.97	77.31±15.66	3.18±0.87	0.06±0.01	0.25
Dorian	3.16 (0.50|0.90|1.76)	2.13	4.43	88.64±22.87	3.51±0.90	0.07±0.01	69.80
Riley	4.16 (0.37|0.76|3.04)	2.39	5.43	59.76±15.91	3.64±0.97	0.04±0.01	19.10
Maria	3.21 (0.40|0.47|2.35)	1.85	4.77	77.71±15.88	3.07±0.90	0.05±0.04	5.25
2013NE	3.64 (0.40|0.46|2.78)	2.02	5.75	75.18±26.41	3.59±0.88	0.08±0.02	25.15

[a] Reference calculation assumes a uniform β_f of 0.1.
[b] Values in parenthesis provide the partitioning of the TWL into its components of tide, surge, and runup.
[c] Approximate total rainfall between the survey dates for the storm given in Table 1. Data from the Advanced Hydrologic Prediction Service (McEnery et al., 2005).

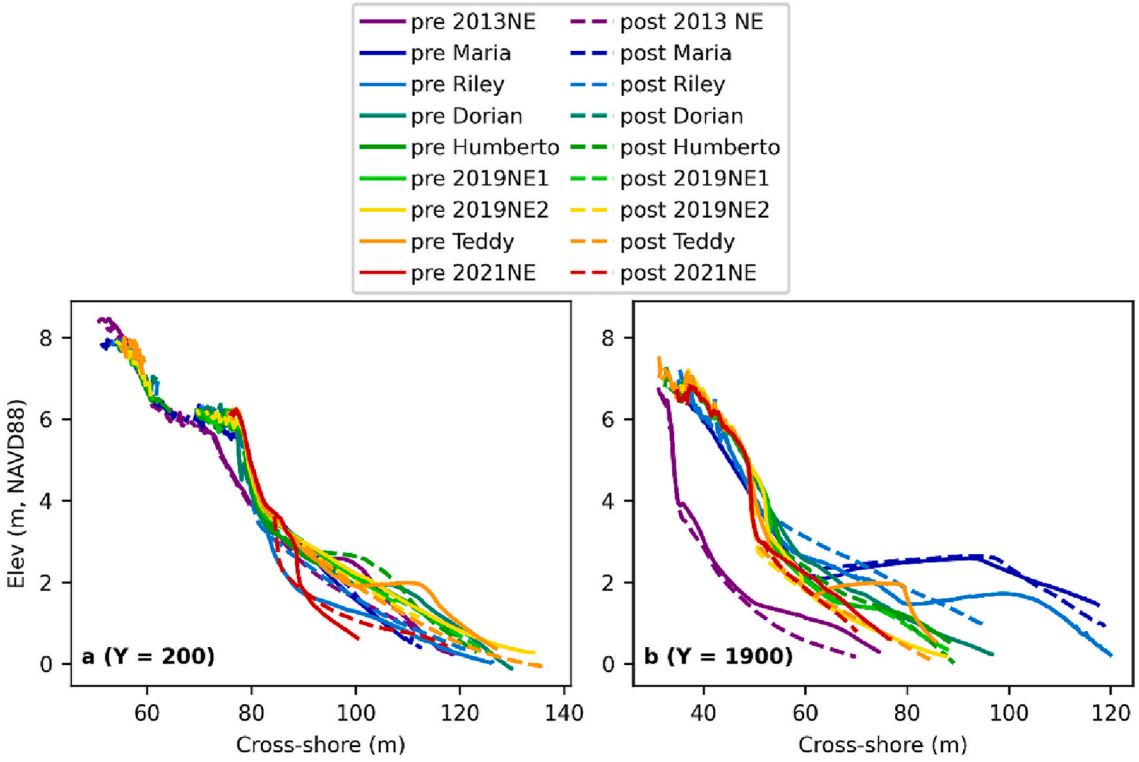

Fig. 4. Pre- and post-storm beach profiles at two longshore positions. (a) Y = 200 and (b) Y = 1900. Mean high water elevation is 0.36 m.

where Maria and Humberto did not result in any zones of dune erosion that met the selection criteria (Fig. 5). Teddy resulted in dune retreat along nearly half of the 4 km study site (Fig. 5a, Table 2). 2019NE2, Dorian, and 2013NE also resulted in dune retreat over more than a total of 1 km, while Riley, 2019NE1, and 2021NE resulted in spatially sparse, but measurable, dune erosion (Fig. 5a, Table 2). Dune retreat occurred in the region Y > 1000 m (managed dune) for five of the seven storms, while dune retreat occurred in Y < 1000 m (unmanaged dune) for three of the seven storms. For two of these three storms (Riley and 2021NE) dune retreat occurred only in the unmanaged dune (Fig. 5a). The region ~Y = 1000–3000 m generally had the most frequent occurrence of dune erosion within the study domain.

Two of the seven storms (Dorian and 2019NE2) resulted in, on average, downward dune retreat ($-\beta_T$), while four resulted in, on average, upward dune retreat ($+\beta_T$) (Fig. 5a, c). All storms show a range of β_T, where interquartile ranges are 36–240 % of medians. Teddy resulted in the largest of these ratios, and is the only storm for which the interquartile range spans 0, though 2019NE2 resulted in the greatest overall β_T interquartile range (0.25 for 1605 m of impacted dune; Fig. 5a, c). Riley and 2019NE1 resulted in the most steeply upward retreat, with median β_T values of ~0.2. For the two storms that drove (on average) downward retreat (Dorian and 2019NE2), median β_T values were −0.07 and −0.26, respectively.

Other morphometrics were also quantified to provide context for the β_T observations, including Z_e and dx_c (Fig. 2). Median Z_e values for all storms ranged from 1.35 m for Dorian to 3.34 m for 2013NE (Fig. 5, Table 3). Notably, the two storms that drove (on average) downward retreat (Dorian and 2019NE2) obtained the two lowest median Z_e values (1.35 m for Dorian and 1.68 m for 2019NE2; Fig. 5, Table 3). Likewise, these two storms also obtained the lowest median dx_c values at −3.61 m for Dorian and −2.83 m for 2019NE2 (negative indicating landward contour migration). However, three of the remaining five storms, all of which drove on average upwards toe retreat, also obtained negative median dx_c values (Fig. 5, Table 3). These observations suggest that Z_e and dx_c may be dynamically linked to β_T; this is explored further in Section 5.

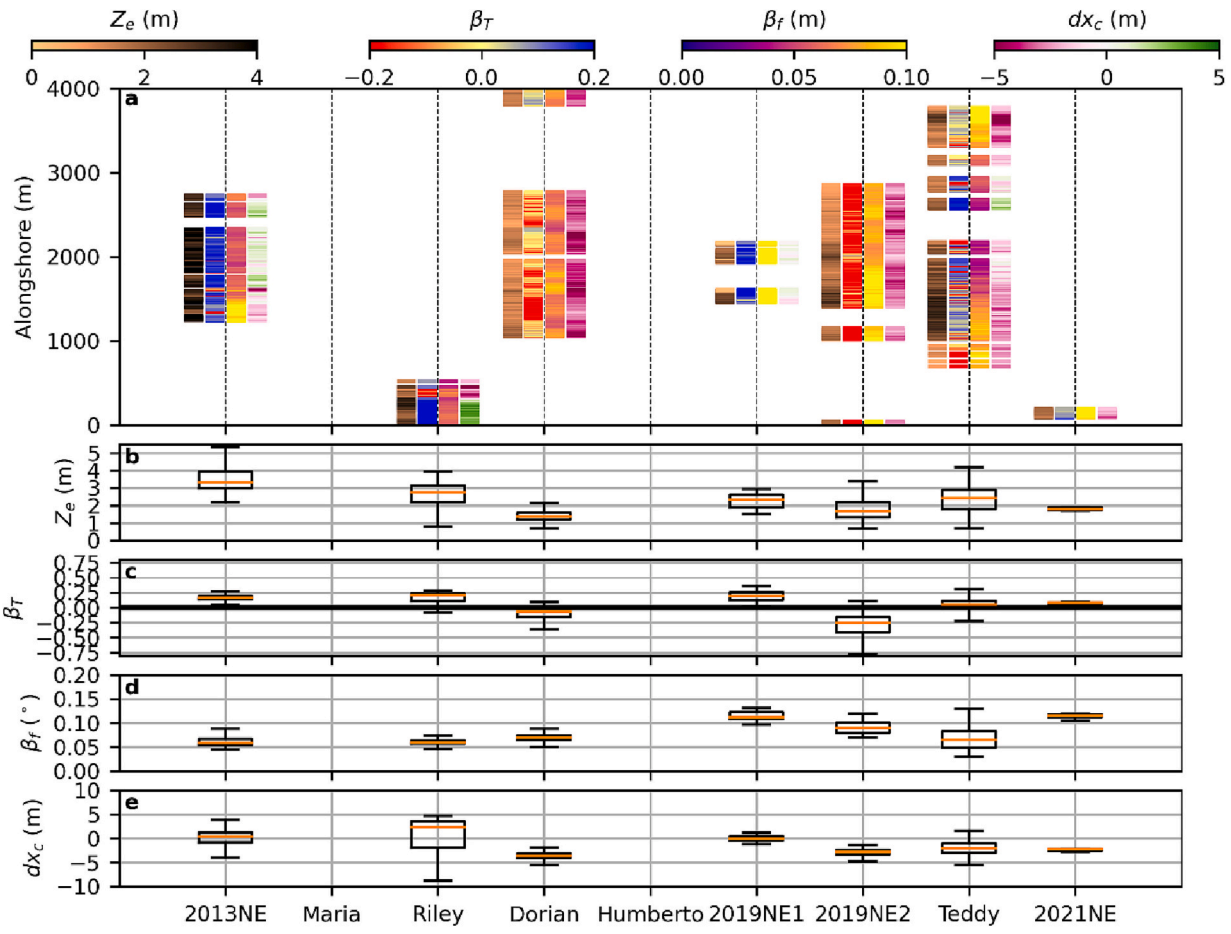

Fig. 5. Summary of dune changes. (a) Space-time plot where extracted regions of dune retreat are colored by Z_e, β_T, β_f, and dx_c. (b–e) Box plots for the distributions of these four parameters for each storm for which dune retreat was observed. Outliers are not plotted.

Table 3
Summary of dune response morphometrics for each storm.

	Median β_T [a]	Median dx_c [a]	Median Z_e [a]	Eroded length (max = 4000 m)
2021NE	+0.08	−2.35	1.81	105
Teddy	+0.05	−2.09	2.41	1980
2019NE2	−0.26	−2.83	1.68	1605
2019NE1	+0.19	−0.05	2.34	335
Humberto	N/A	N/A	N/A	0
Dorian	−0.07	−3.61	1.36	1885
Riley	+0.21	+2.32	2.75	480
Maria	N/A	N/A	N/A	0
2013NE	+0.16	+0.36	3.34	1075

[a] Median values are calculated only within the regions where dune retreat was identified.

4.3. Dune retreat trajectory in relation to total water level

The comparison of $F_{T,m\%}$ and β_T in Fig. 6 indicates a non-linear relationship exists, at all exceedance levels both for all observations and for bulk average values generated during each storm. β_T values for the smallest $F_{T,m\%}$ are strongly negative (steeply downward retreat), whereas β_T values for the largest $F_{T,m\%}$ may asymptotically approach a maximum positive value (upward retreat; Fig. 6a–f). Additionally, $TWL_{7\%}$ most effectively differentiates instances of downward and upward dune toe retreat; that is, on average, $F_{T,7\%} = 0$ separates storms with $-\beta_T$ from storms with $+\beta_T$ with only one storm (Teddy) not following this pattern (Fig. 6d). In comparison, for $F_{T,2\%}$, 2/7 storms (those with $-\beta_T$) are not differentiated by $F_{T,2\%} = 0$ because all storms show on average positive $F_{T,2\%}$ (Fig. 6b), indicating that occasional swash (e.g., 2 % of the swash maxima) exceeded Z_{Toe} on average for all storms that caused dune erosion. For $F_{T,16\%}$, 3/7 storms (all with $+\beta_T$) are not differentiated by $F_{T,16\%} = 0$ (Fig. 6f).

The comparison of $t_{I,m\%}$ and β_T in Fig. 6 shows similar patterns to those of $F_{T,m\%}$. Consistent with the non-linear relationship between β_T and $F_{T,m\%}$, in general, storms with $-\beta_T$ have relatively small values of $t_{I,m\%}$ (i.e. small impact durations) whereas those with $+\beta_T$ show larger values of $t_{I,m\%}$ (i.e. longer impact durations) that asymptote to a maximum value (Fig. 6g–l). Differing slightly from the relationship with $F_{T,m\%}$, however, $R_{2\%}$ and $R_{7\%}$ differentiate equally well cases of downward and upward retreat in terms of $t_{I,m\%}$. For both, storms with $-\beta_T$ show $t_{I,m\%}$ near zero and storms with $+\beta_T$, except for Teddy, show appreciably larger $t_{I,m\%}$ (>15 h for $t_{I,2\%}$ and >2 h for $t_{I,7\%}$). For $t_{I,16\%}$ on the other hand, two additional storms with on average $+\beta_T$ show $t_{I,16\%}$ near zero. For higher TWL exceedance levels, corresponding to lower TWL elevations, the amount of time for which those elevations exceed Z_{Toe} decreases for all storms. The highest TWL exceedance level (lowest TWL elevation) of $R_{16\%}$ (i.e. $TWL_{16\%}$) reached above Z_{Toe} for only two storms (2019NE1 and 2021NE), both of which experienced, on average, $+\beta_T$ (upward toe retreat; Fig. 6l).

Given that $F_{T,m\%}$ and $t_{I,m\%}$ are not independent of one another, as both depend on the extracted Z_{Toe} and corresponding β_f, it is not surprising that their relationships with β_T are similar. However, as represented in Fig. 7, the relationship is not uniform for all storms. While most storms follow a similar exponential relationship for $0 \leq F_{T,2\%} \leq 2$, 2013NE and Dorian are anomalous. 2013NE exhibits a relatively large $t_{I,2\%}$ for a given $F_{T,2\%}$. This indicates that elevated water levels, which

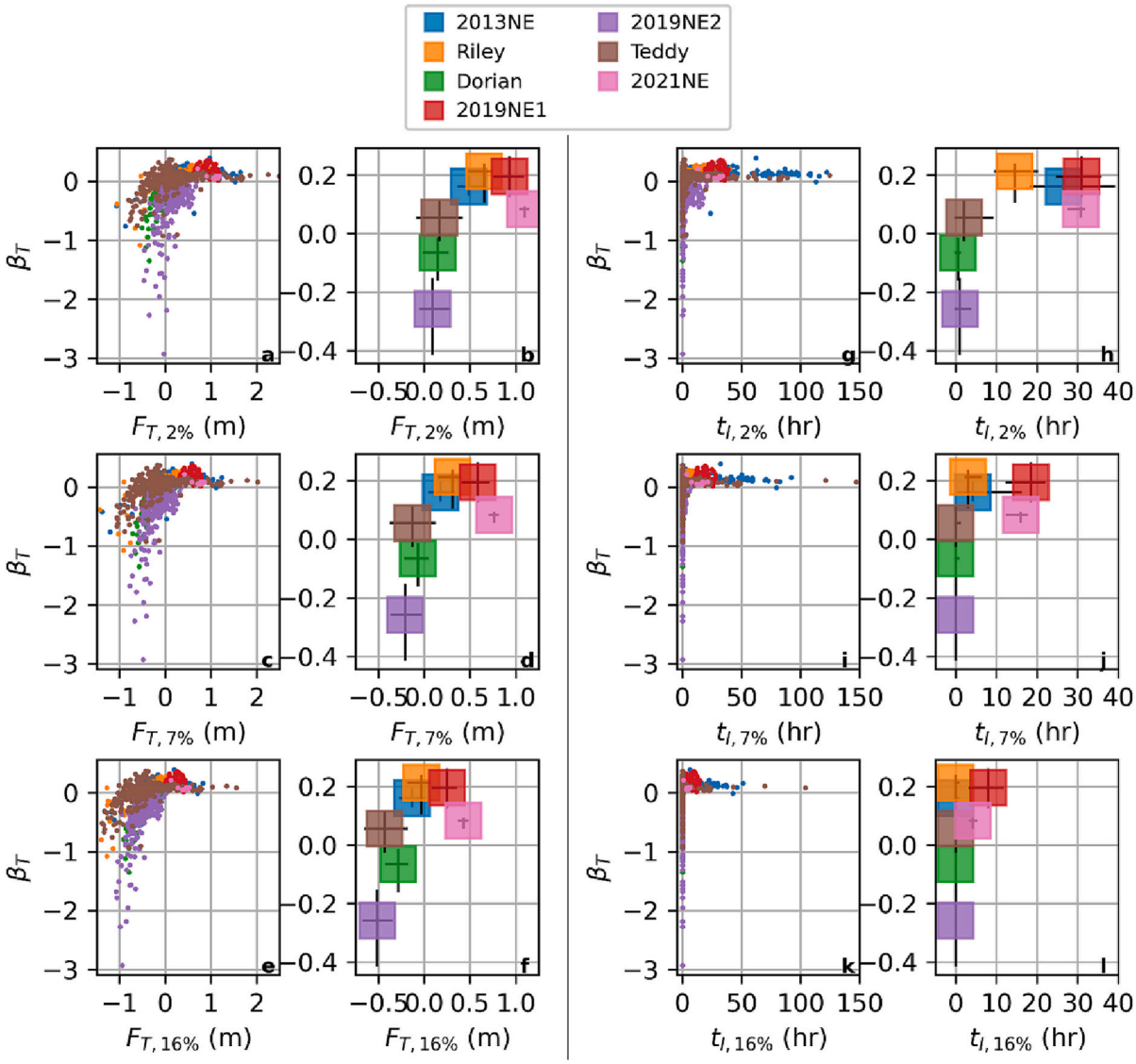

Fig. 6. Scatter plots of dune toe retreat trajectory vs. dune toe freeboard (a–f) and dune toe retreat trajectory vs. impact duration (g–l) for different total water level exceedance levels. In each section, left column shows plot for a given total water level exceedance value for all profiles, right column shows storm-averages, where the box center is at the median values and bars extend to the interquartile ranges.

were higher (relative to Z_{Toe}) than for all storms except Teddy, remained high for a relatively long duration. In contrast, Dorian exhibits a relatively small $t_{I.2\%}$ for a given $F_{T.2\%}$, indicating that water levels remained elevated (relative to Z_{Toe}) for a relatively short amount of time during this event.

5. Discussion

Dune retreat was observed in response to seven of the nine storms analyzed in this study. As a function of longshore varying beach slopes (and therefore wave runup) and dune toe elevations (Table 2), some storms, such as Teddy, resulted in dune erosion over the majority of the 4 km site, while others (e.g. Riley) resulted in much more localized regions of dune retreat (Fig. 5). These complex patterns in dune impacts are consistent with the findings of other observational studies focused on quantifying spatial variability in dune volume changes across the Outer Banks, with hotspot dune erosion locations often found to be correlated with steep pre-storm foreshore slopes and/or complex nearshore bathymetry (e.g., Cohn et al., 2021, 2022b). Where dune erosion did occur, the results of this study indicate that *TWL* may be a predictor of the trajectory of dune toe retreat. Below, patterns of dune retreat, β_T, and their relationships with $TWL_{m\%}$ are further discussed.

As illustrated in Fig. 8 and shown for all data in Fig. 9, instances of downward ($-\beta_T$) and upward ($+\beta_T$) dune retreat are generally associated with different styles of both dune erosion and beach change. Upward dune toe retreat typically coincides with erosion of the dune face (i.e. erosion to a higher Z_e) and sometimes deposition of material at and around the pre-storm dune toe, ultimately leading to a relatively small retreat (or even advance) of the pre-storm dune toe contour (small negative or positive dx_c) and often (though not always) an increase in β_f (Fig. 8, 9). Conversely, downward dune retreat typically coincides with scour just above and below the pre-storm toe without substantial erosion of the dune face (small Z_e), though a vertical scarp at the base of the dune is regularly developed (Fig. 8b). Associated with the downward erosion of Z_{Toe}, there is typically also a reduction in β_f and strong retreat of the pre-storm dune toe contour (large negative dx_c) and erosion of the beach face (Figs. 8, 9). Bonte and Levoy (2015) also observed a linkage between β_T and the beach in front of an artificially created scarp, noting that the vertical change to the fronting beach had an influence on the sign of β_T.

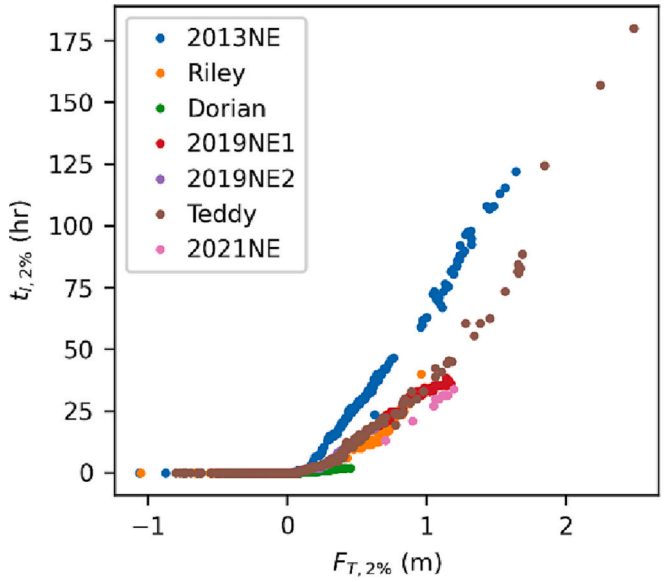

Fig. 7. Dune toe freeboard vs. impact duration for 2 % total water level exceedance level at all transects that experienced dune retreat, where points are colored by storm.

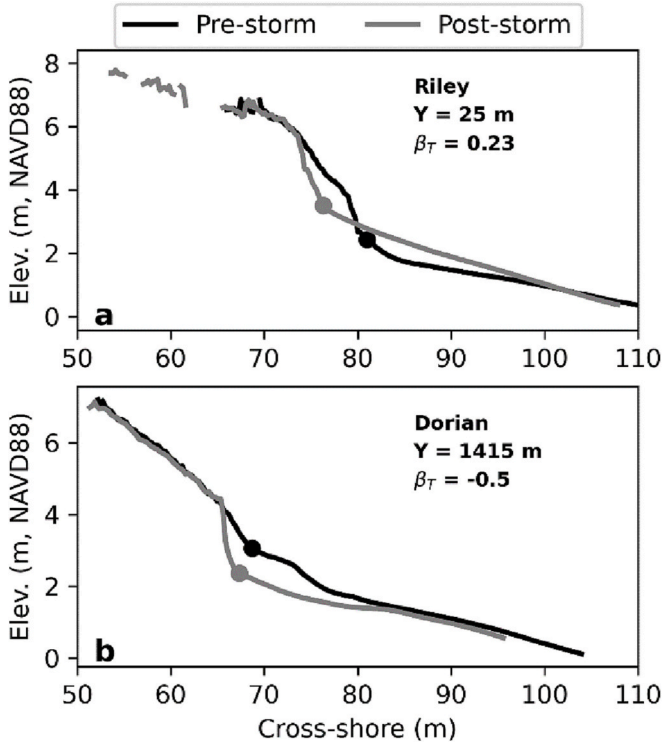

Fig. 8. Example profile evolution for cases of upward (a) and downward (b) dune retreat.

In each case, these couplings between beach and dune changes represent contrasting influences on dune vulnerability. For example, increasing Z_{Toe} for the $+\beta_T$ case will decrease vulnerability to further collisional impacts (Sallenger, 2000), yet a concurrent increase of β_f drives higher wave runup and therefore $TWL_{m\%}$, increasing vulnerability (Stockdon et al., 2006). Conversely, decreasing Z_{Toe} associated with $-\beta_T$ increases vulnerability to further erosion, yet a concurrent decrease of β_f reduces $TWL_{m\%}$ and therefore decreases vulnerability. The role of these simultaneous positive and negative feedbacks on dune collision has important implications for dune vulnerability at the intra-storm timescale, and could be a useful avenue of further research utilizing continuous data streams during storms (e.g., O'Dea et al., 2019; Phillips et al., 2019).

The distinct dune/beach erosion patterns for downward vs. upward dune toe retreat trajectory suggest a possible *TWL* control on β_T, where upward (downward) retreat occurs when $TWL_{m\%}$ is (is not) sufficiently high relative to Z_{Toe}, for sufficient duration, to cause dune face erosion. This is consistent with the observed nonlinear relationships between $F_{T,m\%}$, $t_{I,m\%}$ and β_T (Fig. 6). Interestingly, while the very highest water levels (those from the $TWL_{2\%}$ calculations) were above Z_{Toe}, on average, for all storms, $TWL_{7\%}$ and $TWL_{16\%}$ are more effective at discriminating upward vs. downward retreat in terms of $F_{T,m\%}$ (Fig. 6a–f), which could reflect a hydrodynamic control. That higher *TWL* exceedance values of $TWL_{7\%}$ and $TWL_{16\%}$ are more effective at discriminating upward vs. downward retreat (Fig. 6a–f) could indicate that the sign of β_T is influenced more by surf zone-type processes of wave breaking-induced turbulence, undertow than by extreme swash uprush/backwash, represented by $TWL_{2\%}$. This is consistent with Palmsten and Holman (2012), who found $R_{16\%}$ to be a better predictor of dune erosion than $R_{2\%}$ in a lab experiment, as well as the role of the DSWL, which sets the location of wave breaking, in being a potentially important predictor of spatial patterns in dune erosion (Cohn et al., 2019).

While relationships between $t_{I,m\%}$ vs. β_T are similar to those of $F_{T,m\%}$ vs. β_T (Fig. 6), the relationship between $t_{I,m\%}$ and $F_{T,m\%}$ is not consistent for all storms (Fig. 7). Both $t_{I,7\%}$ and $t_{I,2\%}$ effectively discriminate, on average and with the exception of Teddy, upward vs. downward retreat, whereas $F_{T,2\%}$ is not as effective as $F_{T,7\%}$ (Fig. 6g–l). In other words, while the height of less extreme water levels (e.g. $F_{T,7\%}$) effectively predicts the trajectory of dune toe retreat, the duration for which the most extreme water levels impact the dune ($t_{I,2\%}$) does so as well. Importantly, $t_{I,m\%}$ captures information about the time-history of water levels that $F_{T,m\%}$ does not, providing a possible explanation for this difference. Given that $R_{7\%}$ effectively differentiates, with the fewest number of incorrect categorizations, the sign of β_T for both $F_{T,7\%}$ and $t_{I,7\%}$ (with Teddy being the incorrect storm), it may be more suitable than extreme swash (e.g., $R_{2\%}$, R_{max}) for predicting β_T at this site and should be further tested at other sites.

A survey of previous studies investigating dune erosion in laboratory and field settings have found a range of β_T values, both positive (Palmsten and Holman, 2012; Splinter and Palmsten, 2012; Bonte and Levoy, 2015) and negative (Splinter and Palmsten, 2012; Overbeck et al., 2017). However, the mechanisms controlling this range in values have not previously been widely explored. The range in β_T values found in the present study is consistent with the wide scatter in potential β_T found in the literature. However, the data from these collective datasets generally indicate that β_T is nearly always constrained to values lower than 0.3 and is often much lower, particularly in cases where $F_{T,2\%}$ is near zero (Fig. 10). An exponential fit to all these data of the form $y = a^{b-x} + c$, constrained to $F_{T,m\%} > 0$ to conform with the conventional SIS framework that dune retreat cannot occur without collision (e.g. Sallenger, 2000), achieves an R^2 value of 0.27 (Fig. 10a). The c parameter represents the upper limit β_T value as $F_{T,2\%}$ becomes large (>2 m), and obtains a value of 0.17, which is consistent with the lack of larger positive values of β_T in other field observations (Fig. 10a). Though values of $F_{T,7\%}$ are not typically reported, a similar relationship is found using the data from this study alone, with an R^2 value of 0.21 and upper limit of $\beta_T = 0.16$ (Fig. 10b). Despite the trends found here, scatter in the available β_T data (e.g., Fig. 10) suggests that highly local, spatially variable physical factors such as (1) grain size effects on local slopes (e.g., McFall, 2019), (2) influence of geotechnical properties on sediment mobility, (3) biomass controls on dune erodibility and wave reflection off the dune face (e.g., Feagin et al., 2023; Stark, 2023), (4) groundwater and moisture effects on avalanching processes (Palmsten and Holman, 2011; Conti et al., 2023; Davis et al., 2023), and (5) 2D topographic and

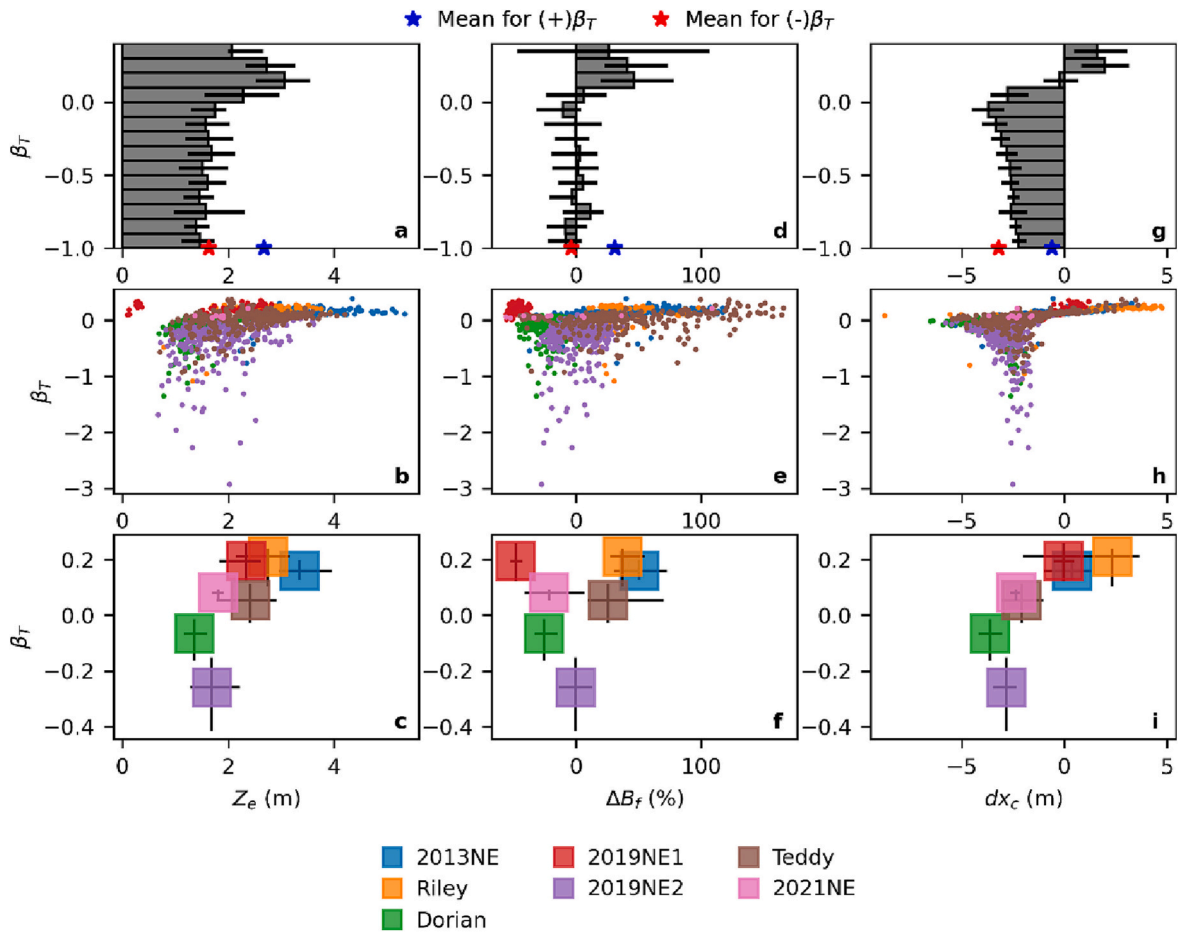

Fig. 9. Relationships for all profiles that experienced dune retreat between the dune toe retreat trajectory and (a–c) the maximum elevation of retreat, (d–f) change in beach-face slope, and (g–i) the cross-shore position change of the pre-storm dune toe elevation contour. For each column, first row shows binned values, where wide bars extend to medians with the interquartile range given with the thin bars; second row shows a scatter plot for all values; and third row shows storm-averaged values, where the box is at the median values and bars extend to the interquartile ranges.

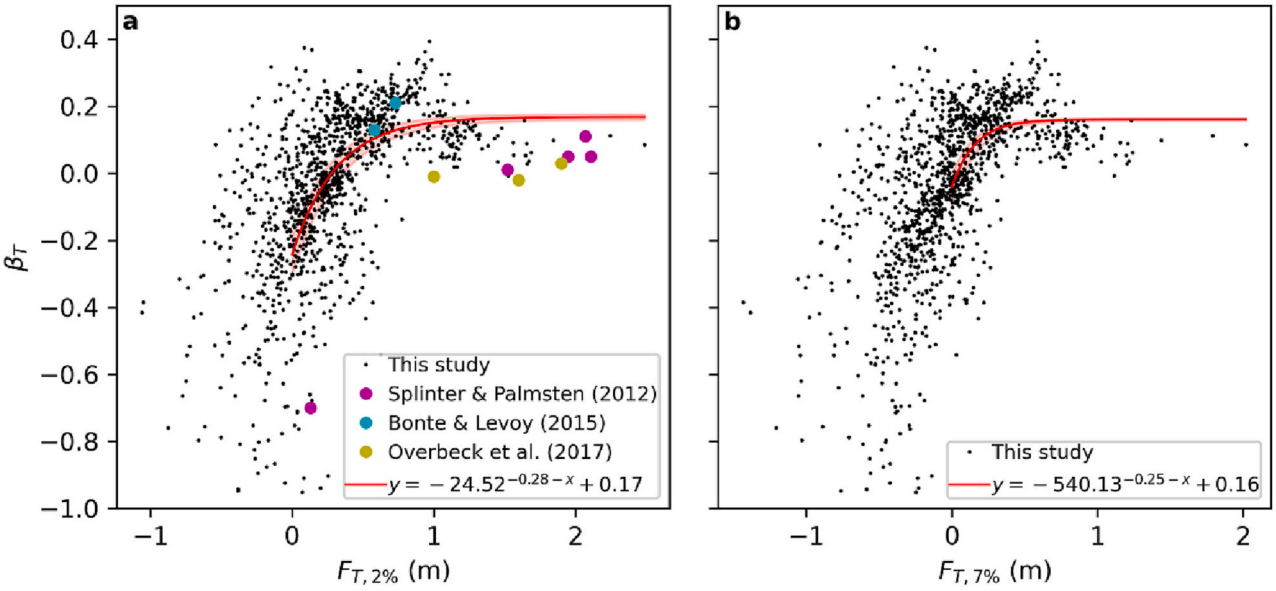

Fig. 10. Dune toe retreat trajectory vs. (a) dune toe freeboard with $TWL_{2\%}$ and (b) dune toe freeboard with $TWL_{7\%}$, for this and other studies. Exponential fits are also plotted, with 99 % confidence bounds shaded. Note that the lower y-axis limit is capped at −1 to aid visual interpretation; 0.08 % of observations obtained $\beta_T < -1$, with a minimum value of −3.

bathymetric effects on wave focusing and runup (Cohn et al., 2021; Kim et al., 2023) may influence these trajectory patterns. This encourages the need for additional detailed datasets of dune retreat at the storm timescale to inform the relative importance of each of these mechanisms for influencing the style of dune retreat. β_T. Additionally, the composition of *TWL* in terms of tide, surge, and runup can have implications for dune response; the height of the DSWL, for instance, dictates the amount of short wave energy that reaches the dune toe (Cohn et al., 2019). An examination of Tables 2 and 3 reveals that there may be some evidence that dune change morphometrics are negatively correlated to surge, though this requires further exploration.

A physical justification for an upper limit of β_T is provided by the fact that the pre-storm dune slope is a plausible β_T maximum, since to exceed this value would require the post-storm toe to be seaward of the pre-storm dune face (yet landward of the pre-storm toe). The pre-storm dune slope averages 0.42 as estimated from the position of the dune toe to Z = 5 m from the available lidar datasets. The fact that the observed upper limit to the fit of β_T (~0.17) is considerably lower than this theoretical β_T limit (~0.42) reflects that such steep upward retreat is not likely in natural dune systems. Similarly, occurrences where $F_{T,7\%} > 0$ are nearly always accompanied by $\beta_T > 0$, indicating that Z_{Toe} rarely remains constant within a single event and that high wave energy (needed to reach the dune face) is likely to drive $+\beta_T$. It remains unclear, as of yet, whether this observed asymptotic limit to β_T is related to angle of repose limitations for saturated sands, morphodynamic controls related to wave and swash reflection off the dune face, or some other unknown feedback effect.

Downward dune toe retreat ($-\beta_T$) is not subject to the same limiters as $+\beta_T$ scenarios. Many of the $-\beta_T$ cases coincided with a scarp formed at the base of the dune. As these scarps often remain near vertical at the storm-timescale (e.g. Fig. 8b) and, in many circumstances, do not result in a drastic landward migration of the cross-shore position of the dune toe (Fig. 9), this allows $-\beta_T$ values to be of larger magnitude than the upper limit on $+\beta_T$ values. The observation that many events where $F_{T,2\%} \leq 0$ drives dune retreat (e.g. Figs. 6, 10) indicates that dunes are not only vulnerable to retreat during events which meet the typical SIS criteria. Interestingly, these erosional, but not formally collisional, events occur nearly exclusively for $-\beta_T$ cases (Figs. 6, 10) suggesting that upper beach erosion can have direct implications for undercutting and subsequent retreat of the dune face. While scarps appear to be commonly developed for $-\beta_T$ trajectories, the potential height of these features is also constrained by saturated conditions resulting from the still water level and groundwater, and/or direct short-wave attack. These forcings are likely to destabilize the feature through slumping and avalanching via capillary action and/or basal wave-cut notches (Nishi et al., 1995; Nishi and Kraus, 1996; Palmsten and Holman, 2011; Davidson et al., 2020). Given that upper beach and dune scarps are prevalent features in coastal systems (e.g., van Bemmelen et al., 2020), are hazards for public safety and for biota (e.g., Rivas et al., 2016), and their formation would not currently be predicted by the SIS for cases where $F_{T,2\%} \leq 0$, furthering our understanding of beach-dune couplings that drive $-\beta_T$ is critical.

Finally, it is noteworthy that our findings are consistent with the conclusions of Overbeck et al. (2017), who suggested that a simple relationship between β_T and β_f (i.e. not considering environmental factors) is not universally applicable across different storms and beach types. Indeed, our observations do not provide evidence of a simple linear relationship between β_T and β_f either ($R^2 = 0.06, p < 0.01$ for all data and $R^2 = < 0.01, p = 0.89$ for storm-averages; not shown). Fig. 10 suggests that an exponential relationship in terms of $F_{T,m\%}$, which is physically grounded and mechanistically corroborated by differences in beach/dune change as a function of *TWL*, could provide a more effective parameterization for β_T in dune erosion models. This relationship is consistent with data from different locations in terms of $F_{T,2\%}$, and is also similar in terms of $F_{T,7\%}$, the metric shown herein to be most suitable for predicting β_T (Fig. 6).

Future work could incorporate the new formulation into existing wave impact dune erosion models to quantify accuracy improvement when comparing with observations. β_T has direct implications on the magnitude of dune volume losses and the distance of expected dune retreat at the storm timescale, thus incorporating a more representative definition of dune toe morphodynamics into predictive tools has the potential to improve forecasting of coastal change hazards that threaten coastal infrastructure and ecosystems. Additionally, the recognition of downward toe retreat under barely collisional events suggests that it is not only the most extreme TWL events that can cause major dune retreat; incorporation of these new formulations into dune retreat models could serve to identify times and locations where dune erosion hazards may exist even when there is limited formal dune collision. Given recent efforts for robust predictions of TWL at regional to national scales (e.g.., Stockdon et al., 2023), there is also the ability to scale predictions of dune retreat, including freeboard effects on β_T, with relative ease.

6. Conclusions

This study examined the dune toe retreat trajectory (β_T) in response to nine storm events along a four km stretch of coast along the Outer Banks of North Carolina. Spatiotemporal occurrences of dune retreat were automatically extracted from elevation change maps for each storm derived from mobile terrestrial lidar observations, and dune toe positions were automatically identified from cross-shore profiles. β_T was quantified alongside other morphometrics including the height above the dune toe to which erosion occurred and the horizontal change in position of the pre-storm dune toe contour. β_T values varied in both magnitude and sign over the events, with two storms (Dorian and 2019NE2) causing downward dune toe retreat ($-\beta_T$) on average, and the other five causing upward retreat ($+\beta_T$) on average. Both the *TWL* elevation above the pre-storm dune toe ($F_{T,m\%}$), as well as the duration for which water levels remained above the dune toe ($t_{I,m\%}$), were shown to exhibit a non-linear relationship with the magnitude and sign of β_T. β_T achieves strongly negative values (steep downward retreat) when $F_{T,m\%}$ and $t_{I,m\%}$ are small, but increases and asymptotically approaches a positive (upward retreat) maximum as values of $F_{T,m\%}$ and $t_{I,m\%}$ increase. Tests with *TWL* calculated using different runup exceedance levels indicate that the 7 % exceedance level ($R_{7\%}$) most effectively differentiates, on average, instances of upward vs. downward retreat both in terms of $F_{T,7\%}$and $t_{I,7\%}$. That is, storms with on-average $-\beta_T$ show $-F_{T,7\%}$ and $t_{I,7\%}$ near 0, with only one storm (Teddy) not following this pattern. For $R_{2\%}$ and $R_{16\%}$ two or more storms do not follow this pattern. The fact that the most extreme exceedance level ($R_{2\%}$) does not serve as an adequate trajectory indicator could suggest that the sign of β_T is more strongly controlled by surf-zone processes such as wave breaking-induced turbulence, undertow, and/or sediment saturation than occasional swash uprush/backwash. This non-linear relationship is shown to be consistent with observations from other studies that have previously been presented as disparate when correlated with only beach-face slope. Physically, this relationship is accounted for by the fact that upward (downward) dune retreat coincides with water levels that are (are not) high enough, for long enough, to substantially erode the dune face, resulting in differing profile evolutions including changes in beach slope and pre-storm dune toe contour position. The asymptotic nature of the relationship is justified in part by the fact that, while $-\beta_T$ can show large magnitude when a dune scarp forms, $+\beta_T$ likely cannot exceed the pre-storm dune slope. More process-based insights are needed to better constrain the morphodynamic mechanisms that drive both the asymptotic nature of $+\beta_T$ and the couplings that control $-\beta_T$. The lack of a consistent relationship between β_T and β_f indicates that simple representations of the beach shape alone cannot explain these feedbacks that drive different patterns of dune retreat during storms. Instead, the non-

linear relationship found between β_T and $F_{T,m\%}$ suggests that these trajectories are largely hydrodynamically controlled. A new parameterization developed from the best fit of these data could yield improvements in parametric dune retreat models over the current common assumption of a linear relationship between β_T and β_f.

Supplementary data to this article can be found online at https://doi.org/10.1016/j.geomorph.2023.108826.

Declaration of competing interest

The authors declare that they have no known competing financial interests or personal relationships that could have appeared to influence the work reported in this paper.

Data availability

All environmental data used in this work can be accessed through the FRF THREDDS server at https://chlthredds. erdc.dren.mil/. All CLARIS data can be found at: https://grid.nga.mil/grid/.

Acknowledgements

This work was funded by ERDC's Flood and Coastal Systems R&D program through the Resilience of Coastal Dunes work unit, by NOAA's National Centers for Coastal Ocean Science, Competitive Research Program under award NA19NOS4780175 to ERDC, and by ERDC's Engineering with Nature Program. We thank Kate Brodie, Nick Spore, and Ian Conery for initial collection of the CLARIS datasets used in this work.

References

van Bemmelen, C.W.T., De Schipper, M.A., Darnall, J., Aarninkhof, S.G.J., 2020. Beach scarp dynamics at nourished beaches. Coast. Eng. 160, 103725.
Birkemeier, W.A., 1985. Time scales of nearshore profile changes. In: Coastal Engineering 1984. American Society of Civil Engineers, New York, NY, pp. 1507–1521.
Birkemeier, W., Dolan, R., Fisher, N., 1984. The evolution of a barrier island: 1930–1980. Shore Beach 52, 2–12.
Bonte, Y., Levoy, F., 2015. Field experiments of beach scarp erosion during oblique wave, stormy conditions (Normandy, France). Geomorphology 236, 132–147. https://doi.org/10.1016/j.geomorph.2015.02.014.
Brodie, K.L., Spore, N.J., 2015. Foredune classification and storm response: automated analysis of terrestrial lidar DEMs. In: Wang, P., Rosati, J.D., Cheng, J. (Eds.), The Proceedings of the Coastal Sediments Conference 2015. World Scientific, Singapore, pp. 1–14.
Brodie, K., Conery, I., Cohn, N., Spore, N., Palmsten, M., 2019. Spatial variability of coastal foredune evolution, part A: timescales of months to years. J. Mar. Sci. Eng. 7 (5), 124.
Burroughs, S.M., Tebbens, S.F., 2008. Dune retreat and shoreline change on the Outer Banks of North Carolina. J. Coast. Res. 24 (10024), 104–112.
Burvingt, O., Masselink, G., Russell, P., Scott, T., 2017. Classification of beach response to extreme storms. Geomorphology 295, 722–737. https://doi.org/10.1016/j.geomorph.2017.07.022.
Carter, R., 1980. Vegetation stabilisation and slope failure of eroding sand dunes. Biol. Conserv. 18 (2), 117–122.
Carter, R., 1991. Near-future sea level impacts on coastal dune landscapes. Landsc. Ecol. 6 (1), 29–39.
Castelle, B., Marieu, V., Bujan, S., Splinter, K.D., Robinet, A., Sénéchal, N., Ferreira, S., 2015. Impact of the winter 2013–2014 series of severe Western Europe storms on a double-barred sandy coast: beach and dune erosion and megacusp embayments. Geomorphology 238, 135–148. https://doi.org/10.1016/j.geomorph.2015.03.006.
Castelle, B., Bujan, S., Ferreira, S., Dodet, G., 2016. Foredune morphological changes and beach recovery from the extreme 2013/2014 winter at a high-energy sandy coast. Mar. Geol. 385, 41–55. https://doi.org/10.1016/j.margeo.2016.12.006.
Coco, G., Sénéchal, N., Rejas, A., Bryan, K.R., Capo, S., Parisot, J.P., et al., 2014. Beach response to a sequence of extreme storms. Geomorphology 204, 493–501. https://doi.org/10.1016/j.geomorph.2013.08.028.
Cohn, N., Ruggiero, P., de Vries, S., Kaminsky, G.M., 2018. New insights on coastal foredune growth: the relative contributions of marine and aeolian processes. Geophys. Res. Lett. 45 (10), 4965–4973.
Cohn, N., Ruggiero, P., García-Medina, G., Anderson, D., Serafin, K.A., Biel, R., 2019. Environmental and morphologic controls on wave-induced dune response. Geomorphology 329, 108–128.
Cohn, N., Brodie, K.L., Johnson, B., Palmsten, M.L., 2021. Hotspot dune erosion on an intermediate beach. Coast. Eng. 170, 103998 https://doi.org/10.1016/j.coastaleng.2021.103998.
Cohn, N., Dickhudt, P., Marshall, J., 2022a. In-situ measurement of grain size characteristics within the aeolian saltation layer on a coastal beach. Earth Surf. Process. Landf. 47 (9), 2230–2244. https://doi.org/10.1002/esp.5373.
Cohn, N., Brodie, K., Conery, I., Spore, N., 2022b. Alongshore variable accretional and erosional coastal foredune dynamics at event to interannual timescales. Earth Space Sci. 9 (12), e2022EA002447.
Conlin, M.P., Adams, P.N., Jaeger, J.M., MacKenzie, R., 2020. Quantifying seasonal-to-interannual-scale storm impacts on morphology along a cuspate coast with a hybrid empirical orthogonal function approach. J. Geophys. Res. Earth Surf. 125 (12), e2020JF005617.
Conti, S., Splinter, K., Boothe, E., Djaidiguna, D., Turner, I., 2023. Laboratory study of dune face erosion mechanisms incorporating variable dune porewater moisture content. In: Wang, P., Royer, E., Rosati, J.D. (Eds.), The Proceedings of the Coastal Sediments Conference 2023. World Scientific, Singapore, pp. 609–614.
Davidson, S.G., Hesp, P.A., Silva, G.M.D., 2020. Controls on dune scarping. Prog. Phys. Geogr. Earth Environ. 44 (6), 923–947.
Davis, E.H., Cohn, N., Heminway, S.S., Skaden, J., Hein, C.J., 2023. Linking internal coastal foredune moisture dynamics to erosion vulnerability. In: Wang, P., Royer, E., Rosati, J.D. (Eds.), The Proceedings of the Coastal Sediments Conference 2023. World Scientific, Singapore, pp. 656–669.
De Winter, R.C., Gongriep, F., Ruessink, B.G., 2015. Observations and modeling of alongshore variability in dune erosion at Egmond aan Zee, the Netherlands. Coast. Eng. 99, 167–175.
Dissanayake, P., Brown, J., Wisse, P., Karunarathna, H., 2015. Effects of storm clustering on beach/dune evolution. Mar. Geol. 370, 63–75.
Dolan, R., Davis, R.E., 1992. An intensity scale for Atlantic coast northeast storms. J. Coast. Res. 8 (4), 840–853. https://www.jstor.org/stable/4298040.
Dolan, R., Davis, R.E., 1994. Coastal storm hazards. J. Coast. Res. SI 12, 103–114.
Dolan, R., Lins, H., Haydena, B., 1988. Mid-Atlantic coastal storms. J. Coast. Res. 4 (3), 417–433.
Drius, M., Jones, L., Marzialetti, F., de Francesco, M.C., Stanisci, A., Carranza, M.L., 2019. Not just a sandy beach. The multi-service value of Mediterranean coastal dunes. Sci. Total Environ. 668, 1139–1155.
Durán, O., Moore, L.J., 2013. Vegetation controls on the maximum size of coastal dunes. Proc. Natl. Acad. Sci. 110 (43), 17217–17222.
Feagin, R.A., Figlus, J., Zinnert, J.C., Sigren, J., Martínez, M.L., Silva, R., et al., 2015. Going with the flow or against the grain? The promise of vegetation for protecting beaches, dunes, and barrier islands from erosion. Front. Ecol. Environ. 13 (4), 203–210.
Feagin, R.A., Innocenti, R.A., Bond, H., Wengrove, M., Huff, T.P., Lomonaco, P., Tsai, B., Puleo, J., Pontiki, M., Figlus, J., Chavez, V., 2023. Does vegetation accelerate coastal dune erosion during extreme events? Sci. Adv. 9 (24), eadg7135.
Fernandez, G.B., Bulhões, E., da Rocha, T.B., 2011. Impacts of severe storm occurred in April 2010 along Rio de Janeiro coast, Brazil. J. Coast. Res. SI 64, 1850–1854.
Frank, P.A.. Ecology and Conservation of the Anastasia Island Beach Mouse (*Peromyscus polionotus phasma*). Retrieved from Proquest. https://www.proquest.com/docview/304312385?pq-origsite=gscholar&fromopenview=true (Doctoral dissertation).
Héquette, A., Ruz, M.H., Zemmour, A., Marin, D., Cartier, A., Sipka, V., 2019. Alongshore variability in coastal dune erosion and post-storm recovery, northern coast of France. J. Coast. Res. 88 (SI), 25–45.
Houser, C., Hapke, C., Hamilton, S., 2008. Controls on coastal dune morphology, shoreline erosion and barrier island response to extreme storms. Geomorphology 100 (3–4), 223–240. https://doi.org/10.1016/j.geomorph.2007.12.007.
Houser, C., Wernette, P., Weymer, B.A., 2018. Scale-dependent behavior of the foredune: implications for barrier island response to storms and sea-level rise. Geomorphology 303, 362–374.
Jackson, N.L., Nordstrom, K.F., 2020. Trends in research on beaches and dunes on sandy shores, 1969–2019. Geomorphology 366, 106737. https://doi.org/10.1016/j.geomorph.2019.04.009.
Jackson, D.W., Costas, S., Guisado-Pintado, E., 2019. Large-scale transgressive coastal dune behaviour in Europe during the Little Ice Age. Glob. Planet. Chang. 175, 82–91.
Kim, L.N., Brodie, K.L., Cohn, N.T., Giddings, S.N., Merrifield, M., 2023. Observations of beach change and runup, and the performance of empirical runup parameterizations during large storm events. Coast. Eng. 184, 104357.
Kobayashi, N., 2016. Coastal sediment transport modeling for engineering applications. J. Waterw. Port Coast. Ocean Eng. 142 (6), 03116001.
Larson, M., Erikson, L., Hanson, H., 2004. An analytical model to predict dune erosion due to wave impact. Coast. Eng. 51 (8–9), 675–696.
Lee, G., Nicholls, R.J., Birkemeier, W.A., 1998. Storm-driven variability of the beach-nearshore profile at duck, North Carolina, USA, 1981–1991. Mar. Geol. 148 (3–4), 163–177. https://doi.org/10.1016/S0025-3227(98)00010-3.
Long, J.W., de Bakker, A.T., Plant, N.G., 2014. Scaling coastal dune elevation changes across storm-impact regimes. Geophys. Res. Lett. 41 (8), 2899–2906.
Madsen, A.J., Plant, N.G., 2001. Intertidal beach slope predictions compared to field data. Mar. Geol. 173 (1–4), 121–139. https://doi.org/10.1016/S0025-3227(00)00168-7.
Martínez, M.L., Hesp, P.A., Gallego-Fernández, J.B., 2013. Coastal dunes: human impact and need for restoration. In: Martinez, M.L., Fernandez, J.B.G., Hesp, P.A. (Eds.), Restoration of Coastal Dunes. Springer, Berlin, Germany, pp. 1–14.
Masselink, G., Puleo, J.A., 2006. Swash-zone morphodynamics. Cont. Shelf Res. 26 (5), 661–680.
Masselink, G., van Heteren, S., 2014. Response of wave-dominated and mixed-energy barriers to storms. Mar. Geol. 352, 321–347. https://doi.org/10.1016/j.margeo.2013.11.004.

Maximiliano-Cordova, C., Salgado, K., Martínez, M.L., Mendoza, E., Silva, R., Guevara, R., Feagin, R.A., 2019. Does the functional richness of plants reduce wave erosion on embryo coastal dunes? Estuar. Coasts 42 (7), 1730–1741.
McCarthy, D.F., 1977. Essentials of Soil Mechanics and Foundations. Reston Publishing Company, Virginia, p. 505.
McEnery, J., Ingram, J., Duan, Q., Adams, T., Anderson, L., 2005. NOAA's advanced hydrologic prediction service: building pathways for better science in water forecasting. Bull. Am. Meteorol. Soc. 86 (3), 375–386.
McFall, B.C., 2019. The relationship between beach grain size and intertidal beach face slope. J. Coast. Res. 35 (5), 1080–1086.
McLachlan, A., 1991. Ecology of coastal dune fauna. J. Arid Environ. 21 (2), 229–243.
Mull, J., Ruggiero, P., 2014. Estimating storm-induced dune erosion and overtopping along U.S. west coast beaches. J. Coast. Res. 298 (6), 1173–1187. https://doi.org/10.2112/JCOASTRES-D-13-00178.1.
Nishi, R., Kraus, N.C., 1996. Mechanism and calculation of sand dune erosion by storms. In: Coastal Engineering 1996. American Society of Civil Engineers, New York, NY, pp. 3034–3047.
Nishi, R., Sato, M., Wang, H., 1995. Field observation and numerical simulation of beach and dune scarps. In: Coastal Engineering 1994. American Society of Civil Engineers, New York, NY, pp. 2434–2448.
O'Dea, A., Brodie, K.L., 2019. Spectral analysis of beach cusp evolution using 3D lidar scans. In: Wang, P., Rosati, J.D., Vallee, M. (Eds.), Coastal Sediments 2019: Proceedings of the 9th International Conference. World Scientific, Singapore, pp. 657–673.
O'Dea, A., Brodie, K.L., Hartzell, P., 2019. Continuous coastal monitoring with an automated terrestrial lidar scanner. J. Mar. Sci. Eng. 7 (37) https://doi.org/10.3390/jmse7020037.
Overbeck, J.R., Long, J.W., Stockdon, H.F., 2017. Testing model parameters for wave-induced dune erosion using observations from Hurricane Sandy. Geophys. Res. Lett. 44 (2), 937–945. https://doi.org/10.1002/2016GL071991.
Overton, M.F., Fisher, J.S., 1988. Simulation modeling of dune erosion. In: Coastal Engineering 1988. American Society of Civil Engineers, New York, NY, pp. 1857–1867.
Overton, M.F., Fisher, J.S., Hwang, K.N., 1994. Development of a dune erosion model using SUPERTANK data. In: Coastal Engineering 1994. American Society of Civil Engineers, New York, NY, pp. 2488–2502.
Palmsten, M.L., Holman, R.A., 2011. Infiltration and instability in dune erosion. J. Geophys. Res. Oceans 116, C10030.
Palmsten, M.L., Holman, R.A., 2012. Laboratory investigation of dune erosion using stereo video. Coast. Eng. 60 (1), 123–135. https://doi.org/10.1016/j.coastaleng.2011.09.003.
Phillips, M.S., Blenkinsopp, C.E., Splinter, K.D., Harley, M.D., Turner, I.L., 2019. Modes of berm and beachface recovery following storm reset: observations using a continuously scanning lidar. J. Geophys. Res. Earth Surf. 124, 720–736. https://doi.org/10.1029/2018JF004895.
Psuty, N.P., 2004. The coastal foredune: a morphological basis for regional coastal dune development. In: Martinez, M.L., Psuty, N.P. (Eds.), Coastal Dunes. Springer, Berlin, Germany.
van Rijn, L.C., 2009. Prediction of dune erosion due to storms. Coast. Eng. 56 (4), 441–457.
Rivas, M.L., Tomillo, P.S., Diéguez-Uribeondo, J., Marco, A., 2016. Potential effects of dune scarps caused by beach erosion on the nesting behavior of leatherback turtles. Mar. Ecol. Prog. Ser. 551, 239–248.
Roelvink, D., Reniers, A., Van Dongeren, A.P., De Vries, J.V.T., McCall, R., Lescinski, J., 2009. Modelling storm impacts on beaches, dunes and barrier islands. Coast. Eng. 56 (11–12), 1133–1152.
Sallenger, A., 2000. Storm impact scale for Barrier Islands. J. Coast. Res. 16 (3), 890–895. https://www.jstor.org/stable/4300099.
Saye, S.E., Van der Wal, D., Pye, K., Blott, S.J., 2005. Beach–dune morphological relationships and erosion/accretion: an investigation at five sites in England and Wales using LIDAR data. Geomorphology 72 (1–4), 128–155.
Serafin, K.A., Ruggiero, P., Stockdon, H.F., 2017. The relative contribution of waves, tides, and nontidal residuals to extreme total water levels on US West Coast sandy beaches. Geophys. Res. Lett. 44 (4), 1839–1847.
Smith, A., Houser, C., Lehner, J., George, E., Lunardi, B., 2020. Crowd-sourced identification of the beach-dune interface. Geomorphology 367, 107321. https://doi.org/10.1016/j.geomorph.2020.107321.
Splinter, K.D., Palmsten, M.L., 2012. Modeling dune response to an East Coast Low. Mar. Geol. 329–331, 46–57. https://doi.org/10.1016/j.margeo.2012.09.005.
Splinter, K.D., Carley, J.T., Golshani, A., Tomlinson, R., 2014. A relationship to describe the cumulative impact of storm clusters on beach erosion. Coast. Eng. 83, 49–55. https://doi.org/10.1016/j.coastaleng.2013.10.001.
Spore, N.J., Brodie, K.L., 2017. Collection, Processing, and Accuracy of Mobile Terrestrial Lidar Survey Data in the Coastal Environment (ERDC/CHL TR-17-5). US Army Corps of Engineers, Vicksburg, MS. https://erdc-library.erdc.dren.mil/jspui/bitstream/11681/22189/1/ERDC-CHL%20TR-17-5.pdf.
Stark, N., 2023. An initial geotechnical field investigation of a dune scarp. In: Wang, P., Royer, E., Rosati, J.D. (Eds.), The Proceedings of the Coastal Sediments Conference 2023. World Scientific, Singapore, pp. 647–655.
Stockdon, H.F., Holman, R.A., Howd, P.A., Sallenger, A.H., 2006. Empirical parameterization of setup, swash, and runup. Coast. Eng. 53 (7), 573–588. https://doi.org/10.1016/J.COASTALENG.2005.12.005.
Stockdon, H.F., Sallenger Jr., A.H., Holman, R.A., Howd, P.A., 2007. A simple model for the spatially-variable coastal response to hurricanes. Mar. Geol. 238 (1–4), 1–20.
Stockdon, H.F., Doran, K.J., Thompson, D.M., Sopkin, K.L., Plant, N.G., Sallenger, A.H., 2012. National assessment of hurricane-induced coastal erosion hazards—Gulf of Mexico. In: U.S. Geological Survey Open-File Report 2012–1084 (51 p.).
Stockdon, H.F., Long, J.W., Palmsten, M.L., Van der Westhuysen, A., Doran, K.S., Snell, R.J., 2023. Operational forecasts of wave-driven water levels and coastal hazards for US Gulf and Atlantic coasts. Commun. Earth Environ. 4 (1), 169.
Suanez, S., Cancouët, R., Floc'h, F., Blaise, E., Ardhuin, F., Filipot, J.F., Cariolet, J.M., Delacourt, C., 2015. Observations and predictions of wave runup, extreme water levels, and medium-term dune erosion during storm conditions. J. Mar. Sci. Eng. 3 (3), 674–698.
Vousdoukas, M.I., Almeida, L.P.M., Ferreira, Ó., 2012. Beach erosion and recovery during consecutive storms at a steep-sloping, meso-tidal beach. Earth Surf. Process. Landf. 37 (6), 583–593. https://doi.org/10.1002/esp.2264.
Wright, L.D., Short, A.D., 1984. Morphodynamic variability of surf zones and beaches: a synthesis. Mar. Geol. 56 (1–4), 93–118. https://doi.org/10.1016/0025-3227(84)90008-2.